Title

Single-cell transcriptomic analysis of macaque LGN neurons reveals novel subpopulations

Authors

Shi Hai Sun[1,2*], Kai Renshaw[1,3,*], John S. Pezaris[1,2]

* Equal Contribution

Affiliations

[1]Department of Neurosurgery, Massachusetts General Hospital, Boston, Mass., USA

[2]Department of Neurosurgery, Harvard Medical School, Boston, Mass., USA

[3]Tufts University School of Medicine, Boston, Mass., USA

Conflicts of Interest

The authors declare no competing interests.

Acknowledgments

Supported by Peter and Yayi Pezaris, Don Good, Michael Gersh, NIMA Foundation, NIH EY027888, and the William M. Wood Foundation, Bank of America, Trustee.

Abstract

Neurons in the lateral geniculate nucleus (LGN) provide a pivotal role in the visual system by modulating and relaying signals from the retina to the visual cortex. Although the primate LGN, with its distinct divisions (magnocellular, M; parvocellular, P; and koniocellular, K), has been extensively characterized, the intrinsic heterogeneity of LGN neurons has remained unexplained. With the development of high-throughput single-cell transcriptomics, researchers can rapidly isolate and profile large sets of neuronal nuclei, revealing a surprising diversity of genetic expression within the nervous systems. Here, we analyzed the transcriptomes of individual cells belonging to macaque LGN using raw data from a public database to explore the heterogeneity of LGN neurons. Using statistical analyses, we found additional subpopulations within the LGN transcriptomic population, whose gene expressions imply functional differences. Our results suggest the existence of a more nuanced complexity in LGN processing beyond the classic view of the three cell types and highlight a need to combine transcriptomic and functional assessments. A complete account of the cell type diversity of the primate LGN is critical to understanding how vision works.

Introduction

The lateral geniculate nucleus (LGN) of the thalamus serves as the main relay through which visual information travels from the retina to the cortex (Sherman & Guillery, 2006; Solomon & Lennie, 2007). Within LGN, visual input is segregated both spatially – distinct areas of the visual field correspond to distinct areas of LGN (Chen *et al.*, 1999; Schneider *et al.*, 2004) – and functionally (Schneider *et al.*, 2004; Denison *et al.*, 2014). A bulk of research has focused on determining the precise spatial, functional, and morphological organization of LGN, as a better understanding of LGN's organization can provide insight into visual processing and has important clinical relevance.

In primates, LGN is composed of distinct layers of functionally similar cell types: magnocellular (M), parvocellular (P), and koniocellular (K). Electrophysiological and morphological studies in primates have determined the specific characteristics of these layers: M neurons, which are large and receive input from rod photoreceptors, are well-suited for rapid temporal dynamics and detecting motion; P neurons, receiving input from cone photoreceptors, are attuned to chromatic changes, making them optimal for processing color and form; and less well-defined K neurons receive input from short-wavelength ("blue") photoreceptors (Wiesel & Hubel, 1966; Schiller & Malpeli, 1978; Kaplan & Shapley, 1982; Derrington & Lennie, 1984; Hubel & Livingstone, 1990, 1990; Maunsell *et al.*, 1999; Reid & Shapley, 2002; Tailby *et al.*, 2008).

As methods for electrophysiological investigation improve, evidence has been accumulating for functional heterogeneity within the three primary LGN cell types. For instance, *on*- and *off*-specific responses from the retina are preserved within distinct populations of M, P,

and K cells (Rousso *et al.*, 2016; Ichinose & Habib, 2022). K cells have also been shown to express receptive fields with non-standard features, including orientation sensitivity, contrast suppression, and many others (Solomon *et al.*, 2010; Cheong *et al.*, 2013; Eiber *et al.*, 2018). Lastly, a recent electrophysiological analysis identified visually responsive LGN cells that did not exhibit any M, P, or K functional responses, suggesting a functional complexity beyond the M, P, and K classification (Sun *et al.*, 2024). All this evidence points toward the existence of multiple subpopulations of LGN neurons within M, P, and K cell types.

Most recently, single-cell RNA-sequencing technologies have been developed for transcriptomic profiling that has been used to identify subclasses of cells by comparing the gene expression patterns of a large number of individual cells within a tissue sample (Ståhl *et al.*, 2016; Lowe *et al.*, 2017; Lein *et al.*, 2017). While past attempts to understand the organization of LGN have relied primarily on morphology and electrophysiology, we hope that analyzing the transcriptome of LGN neurons will reveal more details about their organization and roles in visual processing. In this paper, we explore the transcriptomic diversity of macaque LGN neurons using raw data obtained from a published database (Bakken *et al.*, 2021). Statistical analyses of the LGN transcriptomes revealed nine subpopulations of LGN neurons: two magnocellular populations, three parvocellular populations, and four koniocellular populations. We show that these subpopulations differentially express genes, which imply specific functional differences between these putative subclasses. Our results suggest that there is further nuance in the functional organization of LGN that may be reflected in its role in visual processing. Our findings question the completeness of the established model of LGN organization and emphasize the importance of gaining a more comprehensive understanding of the neural populations in this essential visual relay station.

Methods

RNA data

The RNA-seq data consisting of 2,157 macaque nuclei and accompanying metadata were sourced from the Allen Brain Map (Allen Institute for Brain Science, 2022), available at https://portal.brain-map.org/atlases-and-data/rnaseq/comparative-lgn, and originally used in (Bakken *et al.*, 2021). For single-cell/-nucleus processing for RNA sequencing and processing, please see Bakken *et al.* (2018, 2021); Hodge *et al.* (2019); Tasic *et al.* (2018) for the complete details. In summary, nuclei were isolated by Fluorescence-Activated Cell Sorting, enriched for neurons with neuronal markers, processed with SMART-seq v4 (Clontech) and Nextera XT (Illumina), and sequenced on HiSeq 2500 (Illumina). RNA-seq reads were aligned to corresponding genomes using the STAR aligner (Dobin *et al.*, 2013), and samples had a median depth of 1.3 million reads/nucleus.

Data Analysis

Data preprocessing and analyses were performed in R using Seurat v5 (Butler *et al.*, 2018; Stuart *et al.*, 2019; Hao *et al.*, 2024), using the standardized single-cell transcriptomics analysis workflow (Clarke *et al.*, 2021).

Preprocessing

Using the supplied metadata from the Allen Institute for Brain Science (2022) and Bakken *et al.* (2021), low-quality cells (cells that did not pass quality control criteria: <100,000 total reads,

<1,000 detected genes, < 75% of reads aligned to genome, or CG dinucleotide odds ratio > 0.5; Tasic *et al.*, 2018) and genes (e.g., uncharacterized or non-informative genes) were removed from all further analyses. All cells were prelabeled as M, P, K (Kap and Kp), GABA (GABA 1-4), or pulvinar, as defined in the metadata. Since this study is a comparison of LGN M, P, and K cells, GABA and pulvinar cells were removed from further analyses (61% remaining, n = 1309/2157).

Clustering

M, P, and K cell sets were processed separately using cluster analysis to explore the heterogeneity of LGN neurons. Before clustering, the data was preprocessed and normalized using the Seurat function *SCTransform*, which uses analytic Pearson residuals for normalization (Lause *et al.*, 2021; Choudhary & Satija, 2022), with the top 3,000 highly variable genes used for downstream analyses. For batch correction, we used *IntegrateLayers* with *HarmonyIntegration*, which integrates cells from multiple datasets (Korsunsky *et al.*, 2019). The processed data was then dimensionally reduced using principal component analysis (PCA, via *RunPCA*) using 30 principal components (PCs) and uniform manifold approximation and projection (UMAP, via *RunUMAP*; McInnes *et al.*, 2020) with the first 30 PCs. Clustering was performed using *FindNeighbors* with the first 30 PCs and *FindClusters* with the resolution parameter set to 0.8. We used a relatively high clustering resolution parameter to find novel subpopulations. The robustness of the clustering was determined by bootstrapping the clustering process, as described above, 100 times using a random sampling of 80% of the cells for each bootstrap. The confidence score was then calculated as the number of times a given cell was classified into its most common cluster, which ranged from 99% to 100% for all cells.

Differentially expressed genes

Each cluster was profiled through differential gene expression for comparative analysis. Differentially expressed genes/markers (we will use *genes* and *markers* interchangeably) were determined with the Seurat function *FindAllMarkers*, defined with an adjusted *p*-value < 0.05 (Wilcoxon Rank Sum test). We also defined these genes as biologically significant if the $\log_2$ fold change is greater than 1 (i.e., log2FC > 1 and adjusted *p*-value < 0.05). Gene expression profiles were visualized using heat maps (*DoHeatMap*) and dot plots (*DotPlot*). For the gene ontology analysis, ToppGene (https://toppgene.cchmc.org/enrichment.jsp) and the National Center for Biotechnology Information (NCBI) Gene database (https://www.ncbi.nlm.nih.gov/gene/) were used.

Results

We analyzed the transcriptomes of 1,309 nuclei from microdissected, anatomically defined regions of the macaque lateral geniculate nucleus (LGN) using RNA-seq data sources from the Allen Brain Map (Bakken *et al.*, 2021; Allen Institute for Brain Science, 2022). The RNA-seq data was preprocessed by removing low-quality cells and unnecessary genes (see Methods), as per the metadata provided by the Allen Institute (Allen Institute for Brain Science, 2022). Like in Bakken *et al.* (2021), the gene expression was quantified as the sum of intron and exon reads, normalized as counts per million (CPM), and $\log_2$-transformed. Each cell was categorized into one of the predefined clusters (M, P, K) based on the metadata associated with the published data set (Bakken *et al.*, 2021). These cells in their predefined labels are shown in Figure 1A, illustrating the cell-to-cell genetic diversity in a dimensionally reduced UMAP (Uniform Manifold Approximation and Projection; McInnes *et al.*, 2020) plot.

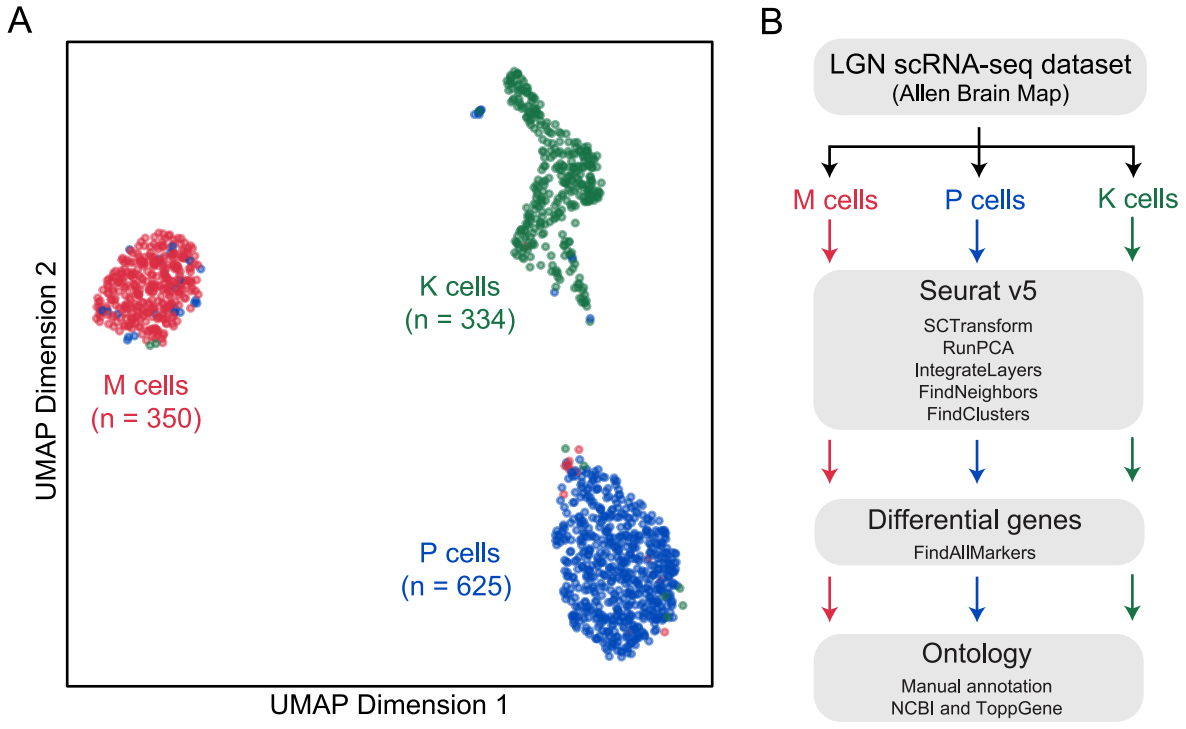

Figure 1. Analysis pipeline of LGN scRNA-seq data, sourced from the Allen Brain Map. **(A)** Scatter plot visualization for each cell (n = 1309) in UMAP space, where the horizontal and vertical axes represent the dimensionality-reduction UMAP coefficients. The magnocellular (M), parvocellular (P), and koniocellular (K) cells are illustrated as red, blue, and green, respectively. **(B)** Flow chart of the analysis pipeline. As labeled in the supplied metadata, sets of the M, P, and K cells were individually preprocessed and clustered with Seurat v5. Differential genes were collected and annotated with each cell population.

Given the wide diversity within primate retinal ganglion cells (Dacey, 2004), and our increasing understanding of the complexity of the LGN (Sun *et al.*, 2024) and the visual cortex (Vries *et al.*, 2020), we believe cellular subtypes within M, P, and K are to be discovered and expect they can be distinguished using transcriptomics. Therefore, for each of the M (n = 350), P (n = 625), and K cells (n = 334) from the publicly sourced dataset, our results will be described below in threefold: (1) how many within-cluster subpopulations (i.e., clusters within M, P, or K sets) are evident in the data; (2) what are the significant genetic differences that define these subpopulations; and (3) what functions and interpretations can we infer using genetic annotation from public resources.

M cell clustering

Two subpopulations emerged from the set of M cells: M_1 (n = 195) and M_2 (n = 155). In Figure 2A, the proximity of the two clusters indicates minimal genetic variance between the M_1 and M_2 populations. The minimal genetic difference between M_1 and M_2 populations could be

attributed to the large number of genes used for the analysis (see Methods). When only considering the significant genes from these populations (*n* genes = 146), the UMAP plot illustrates an ideal separation between the two subpopulations (Figure 2A bottom inset), though we do acknowledge that this report may be considered circular.

The genes that contributed the most to the genetic variance are illustrated in the heatmap of Figure 2B, showing the expression levels of the most differential genes for each cell. However, only one gene, STX1A, was biologically significant (see Methods) between M_1 and M_2 (Figure 2C). STX1A, important for synaptic vesicle docking and neurotransmitter release, had a log2FC of 1.76 and a *p*-value of 0.006. Since the remaining markers had an average gene expression of less than the commonly used 2-fold threshold, the single significant result suggests that the M_1 and M_2 subpopulations we found may not be able to be separated with certainty. This mild level of differentiation is illustrated by the lack of clearly distinct clustering observed in the UMAP plot.

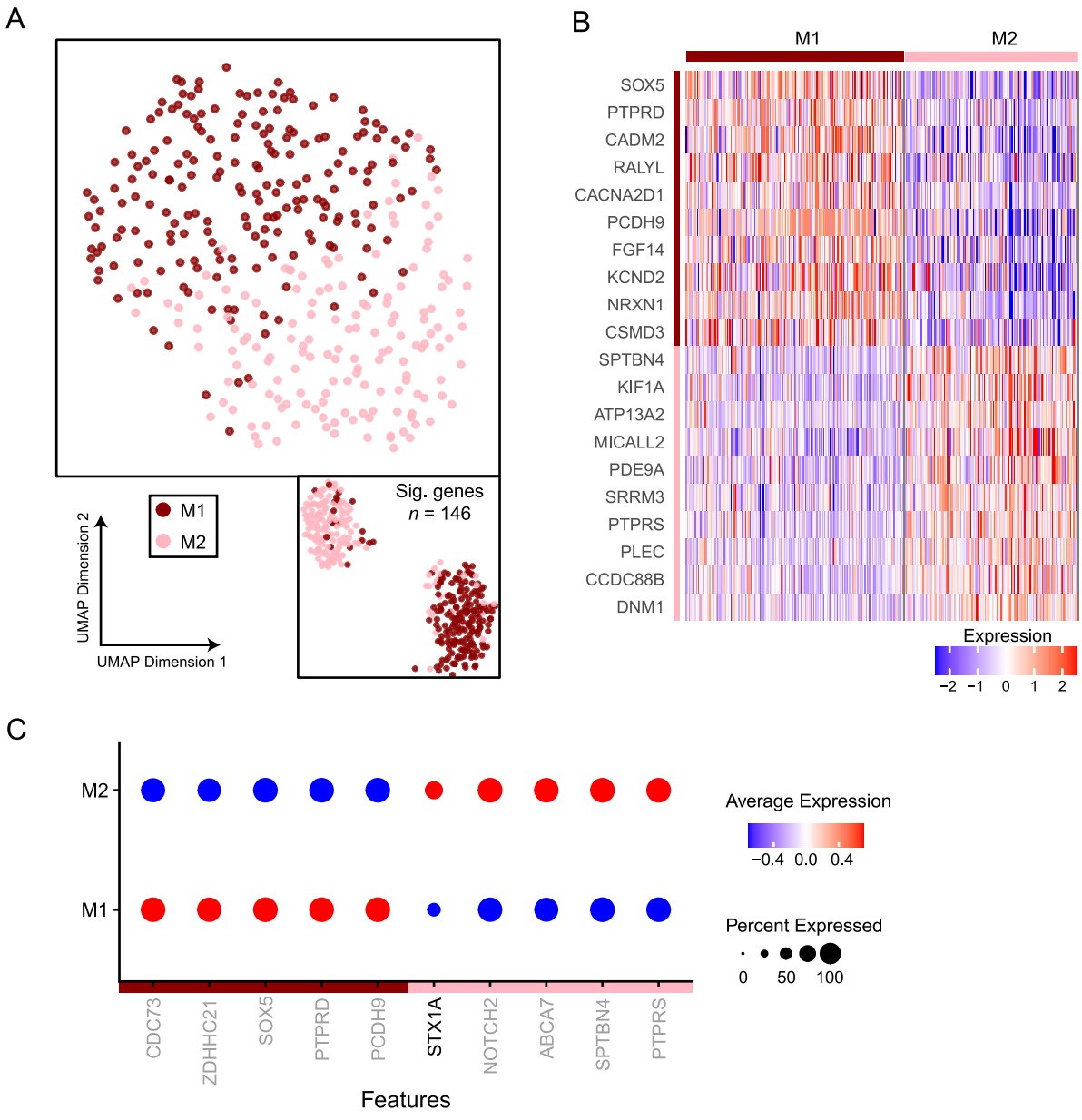

Figure 2. M cell clustering produced two clusters: M_1 (n = 195, magenta) and M_2 (n = 155, pink). (**A**) Scatter plot visualization of M_1 and M_2 clusters in UMAP space for the top features used for clustering (top) and for only the differentially expressed genes between M_1 and M_2 clusters (adjusted *p*-value < 0.05, *n* = 146; bottom). (**B**) Heatmap of RNA-seq expression for the top 10 differentially expressed genes (ordered by increasing adjusted *p*-value; positive fold change only) for each cluster. The horizontal and vertical axes represent individual cells and

differentially expressed genes, respectively. The colored bars at the top and left of the plot represent the cells and the top 10 differentially expressed for each cluster, respectively. The legend at the bottom describes the expression levels for each gene and cell. (**C**) Gene expression dot plot showing the expression of M_1 and M_2 biologically significant markers (adjusted *p*-value < 0.05 and log2FC > 1). Colored bars on the x-axis indicate the genes from M_1 or M_2 cells using the encoding from A. Dot diameter indicates the proportion of cells expressing the gene, and color intensity indicates average expression levels. The grey gene names represent the differential genes that are not biologically significant (see Methods).

Examining the cellular function of gene STX1A, the sole significant differentiator between the M_1 and M_2 subtypes, may suggest potential functional differences. STX1A encodes the SNARE protein syntaxin 1A, which is necessary for neurotransmitter vesicle release. Although there is substantial overlap between syntaxin isoforms, immunohistochemical studies of rat central nervous systems have revealed preferential expression of syntaxin 1A in sensory nuclei, in accordance with our results (Ruiz-Montasell *et al.*, 1996). Most notably, antibodies against syntaxin 1A immunoprecipitated solubilized N-type calcium channels (Südhof, 1995). This interaction between syntaxin 1A and N-type voltage-gated calcium channels may facilitate a fast secretory response to depolarizing action potentials in the M_2 population (Teng *et al.*, 2001). Therefore, the preferential expression of syntaxin 1A in M_2 cells may enable fast response kinetics by this specific M cell population. This functional interpretation is supported broadly by the fact that magnocellular LGN neurons exhibit nonuniform response kinetics. In one study, the response latency within a population of M cells varied by 5–10 ms (Maunsell *et al.*, 1999), indicating variability within the M cell population, which might be partially explained by

variability in SNARE protein expression. However, this heterogeneity in response latency within M cells may also be explained by differences in axon length between ipsilateral and contralateral eyes or other nonspecific inter-cell heterogeneity.

P cell clustering

Three subpopulations of P cells were found: P_1 (n = 246), P_2 (n = 227), and P_3 (n = 152), as seen in Figure 3. P_1 cells consisted of 169 biologically significant markers (see Figure 3C for examples). In contrast, P_2 cells contained only one biologically significant marker, NOTCH2, which is involved in cell differentiation and development, but its specific role in the visual pathway remains unclear. No biologically significant markers were found for P_3; coupled with the minimal marker diversity in P_2, this finding suggests that these two subpopulations may represent a single cellular subtype.

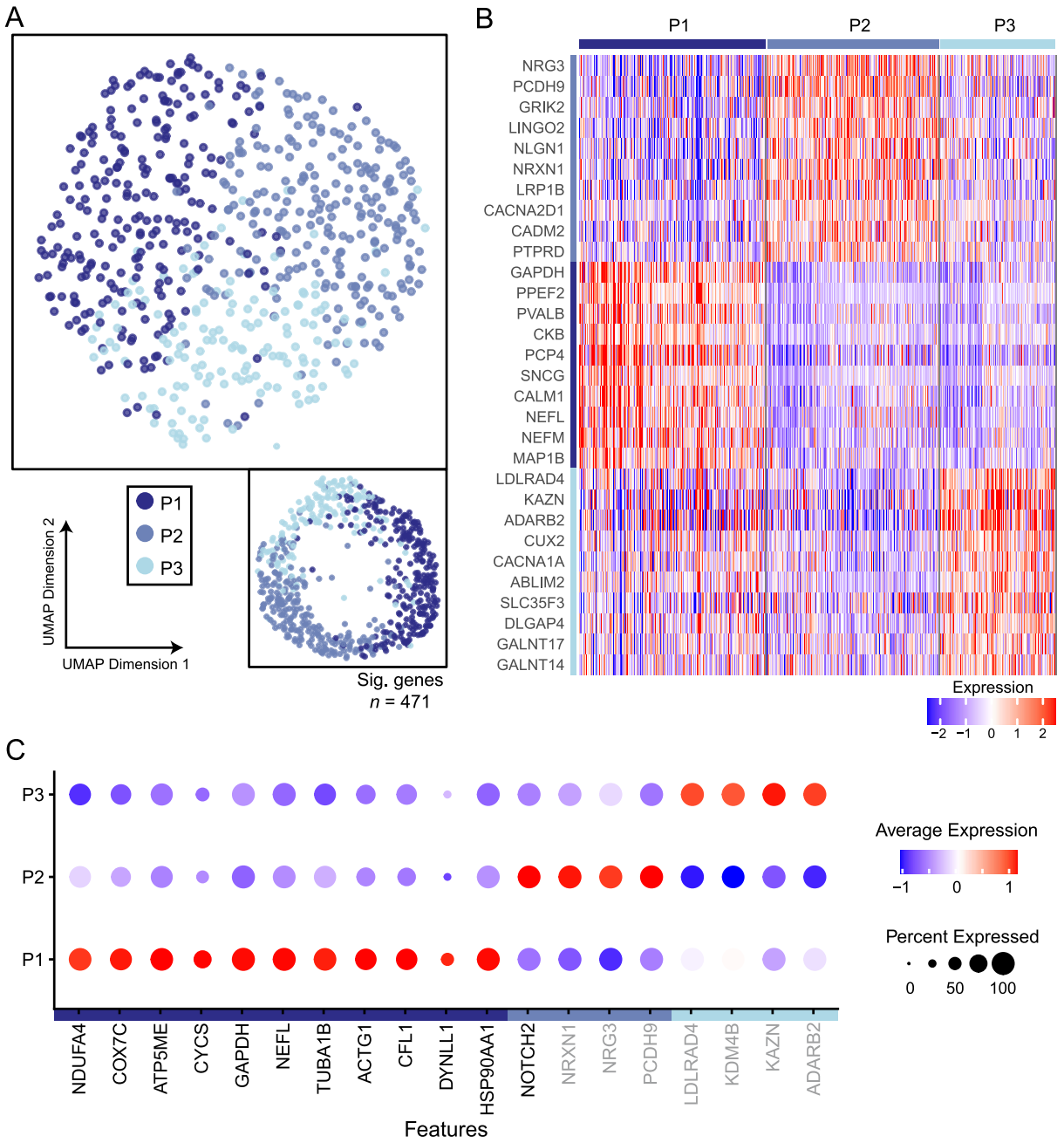

Figure 3. P cell clustering produced three clusters: P_1 (n = 246; dark blue), P_2 (n = 227; medium blue), and P_3 (n = 152; light blue). **(A)** Scatter plot visualization of P_1, P_2, and P_3 clusters in UMAP space for the top features used for clustering (top) and for only the differentially expressed genes (bottom). **(B)** Heatmap of RNA-seq expression for the top 10 markers (adjusted *p*-value < 0.05, ordered by increasing adjusted *p*-value) for each cluster (sectioned by the colored

bars on the left). The horizontal and vertical axes represent individual cells and markers, respectively. The colored bars at the top represent the cells clustered into P_1, P_2, or P_3. The legend at the bottom describes the expression levels for each gene and cell. **(C)** Gene expression dot plot showing the expression of the biologically significant markers from P_1, P_2, and P_3. Colored bars on the x-axis indicate the genes from P_1, P_2, or P_3 cells, with the same encoding as in A. Dot diameter indicates the proportion of cells expressing the gene, and color intensity indicates average expression levels. The grey gene names represent the differential genes that are not biologically significant (see Methods).

The genes preferentially expressed in P_1 cells give substantial insight into the morphology and physiology of this specific subtype. Among the biologically significant markers for P_1 cells were a host of metabolic enzymes and structural proteins. The combination of these proteins' expression suggests that P_1 cells are likely larger, more metabolically active, and may be more electrically active.

Within the significant metabolic enzymes, notable markers include NDUFA4, NDUFS5, NDUFA13, NDUFA11, NDUFA1, NDUFB7, NDUFA3, NDUFB11, NDUFC2 (subunits of complex 1 in the electron transport chain), NDUFB1 (involved in electron transport chain complex 1 assembly), COX8A, COX5A, COX6B1, COX7B, COX7C (subunits of complex 4 in the electron transport chain), ATP5ME, ATP5PD, ATP5PF, ATP5PO (subunits of ATP synthase), ATP5IF1 (enables ATP synthase binding activity), CYCS (cytochrome c), PGK1, TPI1, and GAPDH (glycolytic enzymes; phosphoglycerate kinase, triosephosphate isomerase, and glyceraldehyde-3-phosphate dehydrogenase). The upregulation of metabolic enzymes present in P_1 cells suggests that these cells are more metabolically active than the P_2 or P_3 populations. The

functional relevance of this observation is that P_1 cells may be larger than other P cells (and thus require more metabolic activity) or may be more electrically active than other P cells, or both.

Coexpressed with the numerous metabolic enzymes in P_1 were several neuron-specific structural proteins, further suggesting that these cells are larger and thus have greater energy requirements. Among those structural proteins were two chains of neurofilament (light, NEFL; and medium, NEFM), INA (a neurofilament component associated with NEFM), ACTG1 (gamma isoform of actin), CFL1 (cofilin 1, aids in reorganization of the actin cytoskeleton), DYNLL2, DYNLL1 (dynein light chain, important for moving cargo, such as neurotrophins, neurofilaments, and ribonucleoproteins, from the distal regions of the neuron back to the cell body), TUBB, TUBB4A, TUBB4B, TUBA1A and TUBA1B (tubulin beta and alpha subunits, involved in microtubule cytoskeleton organization). Intuitively, the higher presence of cytoskeletal elements – neurofilament, actin, and microtubules – provides evidence that this population of cells is physically larger – thus requiring greater physical support. Many studies have strongly correlated the expression of neurofilament with neuron size (Lawson & Waddell, 1991; Duffy *et al.*, 2012), axonal diameter (Lasek *et al.*, 1983), and fiber conduction velocity (Lawson & Waddell, 1991). In fact, neurofilament and other structural proteins have been used as markers for M cells, which are known to be larger, with wider axons and faster conduction velocities (Prasad *et al.*, 2002). This raises two interesting possibilities: either this P_1 population is a population of misclassified M cells that coexpress specific P cell markers, or this is a subpopulation of P cells that are morphologically or functionally distinct from the other P neurons.

In addition, many of the genes expressed in the P_1 transcriptome include genes important for maintaining the myelin sheath. Among those genes include many of the structural proteins

listed above (neurofilament and tubulin associated proteins), a group of heat shock proteins (HSPA5, HSPA8, HSP90AA1), and several of the mitochondrial metabolic enzymes listed above. This observation further supports the hypothesis that P_1 cells are a population of larger cells within P, with wider axons and faster propagation velocities. It may also suggest that these cells have improved signal fidelity, as myelin insulates axons, ensuring the signal arrives at the synapse with minimal attenuation (Morell & Quarles, 1999). In the context of the LGN, improved signal fidelity would lead to more faithful transmission of visual information, ultimately contributing to better visual perception.

Taking these hypotheses together, the gene expressions of P_1 cells suggest that these cells are larger, more metabolically active, and perhaps have improved signal fidelity. Given the association between many of these genes and M cells, the possibility that these are misclassified M cells with P-cell-specific markers cannot be ruled out completely. Given that M, P, and K cells are anatomically segregated, future studies that combine anatomic data with spatial transcriptomics can better clarify these results. As for the P_2 and P_3 populations (which may represent a single cellular subtype), it stands to reason that these cells are comparatively smaller and less metabolically active than the P_1 subtype. However, given the limited presence of significant biomarkers in the P_2 and P_3 populations, it is difficult to draw further conclusions about their functionality.

K cell clustering

Among the three principal LGN neuronal types, K cells exhibited the most significant heterogeneity, with four clusters, K_1 through K_4 (n = 100, 129, 63, and 42, respectively), as seen

in Figure 4. The first three subclasses included the strongest transcriptomic signal as well, with 19, 69, and 254 biologically significant markers, respectively, however, K_4 had only 3. Coupled with the minimal marker diversity in K_1, the low number of significant markers in K_4 cells and similarity to the K_1 marker profile (see Figure 4C) suggest that these two classifications may represent a single-cell subtype.

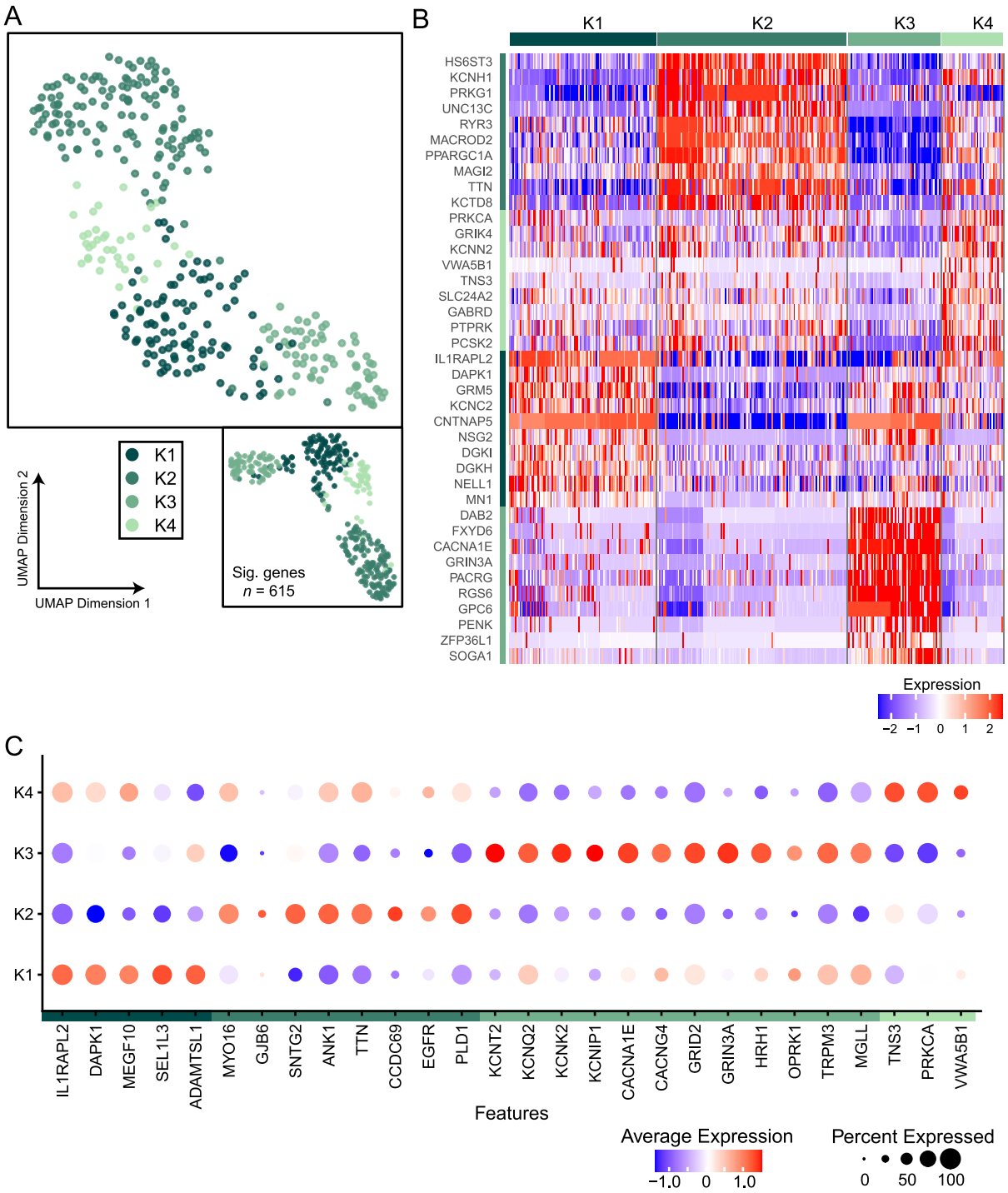

Figure 4. K cell clustering produced four clusters: K_1 (n = 100), K_2 (n = 129), K_3 (n = 63), and K_4 (n = 42), colored from dark green to light green. **(A)** Scatter plot visualization of the K clusters in UMAP space for the top features used for clustering (top) and only the differentially

expressed genes (bottom). **(B)** Heatmap of RNA-seq expression for the top 10 markers (adjusted *p*-value < 0.05, ordered by increasing adjusted *p*-value; with only six markers for K_4 cells) for each cluster (sectioned by the colored bars on the left). The horizontal and vertical axes represent individual cells and differentially expressed markers, respectively. The colored bars at the top represent the cells corresponding to the K clusters. **(C)** Gene expression dot plot showing the expression of the biologically significant markers from K_1 through K_4. Colored bars on the x-axis indicate the genes from each K cluster using the encoding from A. Dot diameter indicates the proportion of cells expressing the gene, and color intensity indicates average expression levels. The grey gene names represent the differential genes that are not biologically significant (see Methods).

The array of markers in the K_1 through K_4 populations reveals interesting features that may reflect functional differences. Given the comparative scarcity of significant biomarkers in the K_1 and K_4 populations, it is challenging to draw functional conclusions for these subtypes, so we will concentrate on K_2 and K_3.

The K_2 population, like the P_1 population, expresses a substantial number of cytoskeletal proteins. However, unlike the P_1 population, which expressed structural constituents of the cytoskeleton, K_2 cells primarily express cytoskeletal binding proteins that bind the cytoskeleton to other cellular elements. These include MYO5B, MYO16 (myosin isoforms), GJB6 (gap junction protein), SNTG2 (syntrophin), ANK1 (ankyrin), TTN (titin), CCDC69 (involved in microtubule binding activity), and TSN1 (tensin), among others. In addition to ankyrin, syntrophin, and gap junction protein (see below) – which bind cytoskeletal elements to intramembranous and extracellular components – K_2 cells also express plasma membrane

proteins involved in cellular recognition and autocrine/paracrine or intercellular signaling (Singh & Harris, 2005; Bruntz *et al.*, 2014; Park & Han, 2018). These include EGFR (epidermal growth factor receptor) and PLD1 (phospholipase D1). The general upregulation of this kind of protein may suggest that interaction with other cells – either via synaptic connections, direct cell-to-cell contact, or autocrine/paracrine signaling – is an important functional component of this cell type.

One additional observation should be made concerning the K_2 population of cells. A highly expressed gene, among many others, in this population was GJB6 (gap junction protein beta 6), which encodes an important connexin protein in gap junctions. The presence of gap junctions in thalamic nuclei, including in LGN, is thought to help synchronize high-threshold action potential bursts, which are presumed to be important for stimulus visibility, attention, and efficient stimulus encoding (Reinagel *et al.*, 1999; Martinez-Conde *et al.*, 2002; Söhl *et al.*, 2005). The expression of this protein, specifically in this K cell subtype, suggests that this cell type may exhibit greater burstiness than other K cell types, perhaps underscoring a distinct role in visual attention, as well as stimulus visibility and encoding.

The K_3 population of cells expresses a large number of monoatomic ion channels, channels important for electrical signaling in nerons. These include KCNIP1, KCNA3, KCNQ2, KCNC4, KCNJ6, KCNK2, KCNK3, KCNH3, KCNT2, KCNK10 (subunits of different potassium channels, including voltage-gated, sodium-activated, two-pore domain, and inwardly rectifying types), CACNA1E, and CACNG4 (voltage-gated calcium channel subunits). In addition to these ion channels, this cell population expresses a substantial amount of neurotransmitter receptors for both glutamate – the primary excitatory neurotransmitter in LGN – as well as other modulatory neurotransmitters. These include GRID2, GRIN3A (glutamate receptors, NMDA and delta type), HRH1 (histamine H1 receptor), OPRK1 (opioid receptor

kappa), MGLL (endocannabinoid related lipase), and TRPM3 (neurosteroid sensitive transient receptor potential channel; Webster, 2019). The increased expression of these genes suggests that this population of cells is highly electrically active and may be the site of visual modulation by non-glutamate neurotransmitter systems within LGN. Each of these points will be considered below.

The electrophysiological implications of the high potassium and calcium ion channel expression are three-fold. First, it suggests enhanced action potential dynamics. Increased expression of voltage-gated potassium channels would enhance the repolarization phase of action potentials, meaning neurons can return to their resting state more quickly after firing (Hodgkin & Huxley, 1952). That would enable them to fire action potentials at higher frequencies, increasing the complexity and potency of transmitted information as well as improving the temporal precision of neural signals. Second, the upregulation of voltage-gated calcium channels may suggest a role in synaptic plasticity, as calcium influx is a key mediator of synaptic plasticity mechanisms such as long-term potentiation (LTP) and long-term depression (LTD) (Weisskopf *et al.*, 1999; Heynen & Bear, 2001; Wankerl *et al.*, 2010). This theory is further supported by the upregulation of the NMDA glutamate receptor (GRIN3A) which is the fundamental receptor type driving LTP and LTD (Collingridge & Bliss, 1987; Nabavi *et al.*, 2013), although voltage-gated calcium channels (such as CACNA1E and CACNG4) have also been associated with these processes (Weisskopf *et al.*, 1999; Wankerl *et al.*, 2010). Finally, the upregulation of potassium and calcium channels may suggest a role in homeostatic regulation and stability by maintaining stable neuronal excitability, preventing excessive firing, and preventing synaptic fatigue during prolonged periods of activity (Bowers & Schmidt, 1992). Functionally, this means that K_3 cells can maintain reliable information transmission under variable stimuli. When compared to K_2

cells, in which the presence of gap junction proteins suggests a propensity for burstiness, it is more likely that K_3 cells maintain stable firing rates across diverse stimuli.

The presence of receptors for non-glutamate neurotransmitters, in turn, suggests that K_3 signals are functionally modulated by other neural systems. These receptors, thus, could be a mechanism for the extra-thalamic shaping of LGN processing. The two most LGN-relevant non-glutamate neurotransmitters – histamine and endocannabinoids – will be considered here.

HRH1 is the H1 histamine receptor. Although the primary role of histamine in the brain is suggested to be related to learning and memory, circadian rhythm, and thermoregulation, studies have found that the presence of histamine in thalamic nuclei (including LGN) may have important neuromodulatory effects. First, a study by Sittig & Davidowa (2001) found that histamine reduces the firing and bursting of thalamic neurons in rats. This finding is in accordance with our hypothesis above on the stable firing rates of K_3 neurons. Second, in LGN specifically, another study found that histamine exerted a depolarizing effect, which was considered important in the control of arousal (Jin *et al.*, 2002). That same study also found that H1 receptors likely act in LGN neurons at their axonal terminus within the cortex, exerting its neuromodulatory effect at the thalamocortical junction. As opposed to those neurotransmitters that modulate retinothalamic transmission, the presence of histamine at the thalamocortical junction suggests that histamine affects higher-order processing, perception, and conscious experience, as opposed to initial sensory processing (Yang *et al.*, 2015; Noseda *et al.*, 2017).

MGLL is a serine hydrolase that plays a critical role in pain and nociception through hydrolysis of the endocannabinoid 2-arachidonoylglycerol. Its presence in K_3 cells and association with the endocannabinoid system may suggest a role for endocannabinoid modulation of vision. A study of the endocannabinoid system in LGN found that

endocannabinoid related proteins, such as receptors, synthesizing enzymes, and degradation enzymes (like MGLL), were expressed primarily in M layers. This was confirmed in our analysis, showing that both M_1 and M_2 cells expressed MGLL. However, they noted an additional weak expression in the K layers (Javadi *et al.*, 2015), consistent with our findings on the K_3 population of cells. The precise function of endocannabinoids in LGN is still poorly understood, but the specificity of this neuromodulation to M and K_3 cells is an interesting observation.

The final remark regarding K_3 cells is the expression of PENK (proenkephalin). Bakken *et al.* (2021) previously performed single-cell RNA sequencing on macaque LGN cells and showed two populations of K cells, Kp and Kap. Kp cells selectively expressed PENK and were enriched in ventral K layers K1 and K2, adjacent to M cells. This association suggests that the K_3 cells we identified were the same Kp cells identified by Bakken et al., or a subpopulation thereof, and may help to explain the commonality in biomarkers between M and K_3 cells. In fact, research in the K1 and K2 layers (where these Kp/K_3 cells are enriched) has shown that these cells demonstrate large receptive fields with sensitivity to contrast and high temporal frequencies – very similar to M cell receptive fields (White *et al.*, 2001; Xu *et al.*, 2001; Solomon *et al.*, 2002).

Discussion

Our analyses revealed nine subpopulations of LGN neurons: two populations of magnocellular neurons (M_1 and M_2), three populations of parvocellular neurons (P_1, P_2, and P_3), and four populations of koniocellular neurons (K_1, K_2, K_3, and K_4). Although the same dataset was used as Bakken *et al.* (2021), our study employed several different analytical methods. For

normalization, we utilized analytic Pearson residuals (*SCTransform*, Lause *et al.*, 2021). To correct for multiple biological and experimental variations, we used *Harmony*, an algorithm that maps cells into a common embedding where they cluster by cell type instead of dataset-specific conditions (*HarmonyIntegration*; Korsunsky *et al.*, 2019). SCTransform and Harmony have demonstrated superior performance to their older counterparts (*SCTransform* vs. log normalization and scaling; *Harmony* integration vs. *FastMNN*) in identifying biologically variable genes. Lastly, we intentionally set the clustering resolution to be relatively high, which poses the risk of overclustering (Clarke *et al.*, 2021). This may be the case for the largely indistinct M_1 and M_2, and P_2 and P_3 clusters reported in this study. However, the remaining clusters revealed novel functional differences between cell populations based on ontology.

The differentially expressed genes between these cell populations imply functional differences between them. Although M_1 and M_2 subpopulations were largely indistinct, they significantly differed in the expression of STX1A, a SNARE protein that may help facilitate a fast secretory response to depolarizing action potentials in M_2 cells. This difference may mean that M_2 cells have faster conduction than M_1 cells, accounting for some of the intrinsic diversity in conduction speed within M cells. P_2 and P_3 subpopulations likewise demonstrated relatively homogenous gene expression, which differed from the gene expression of the P_1 subpopulation. The gene expression of the P_1 cells included many metabolic and structural proteins, leading to the hypothesis that P_1 cells are larger and more metabolically active. Of the four populations of K cells, K_1 and K_4 cells demonstrated relatively similar gene expression, suggesting that these subclasses may not be distinct. It was difficult to conclude the functional specificity of the K_1 and K_4 cells from their significant markers. K_2 cells expressed a host of cytosolic binding proteins, potentially implying a role in intercell communication. In particular, the expression of

gap junction proteins in K_2 cells is associated with the coordination of thalamic bursts, which could be a key feature of K_2 electrophysiology. K_3 cells expressed PENK, the defining characteristic of Bakken *et al.*'s (2021) Kp cells in the two most ventral koniocellular layers. In addition to PENK, K_3 cells highly expressed potassium and calcium ion channel proteins, suggesting enhanced action potential dynamics, synaptic plasticity, and stable firing rates. K_3 cells also express receptors for non-glutamate neurotransmitters, implying that this population may be the target for non-visual modulation of LGN activity. These non-visual inputs may include hypothalamic or brainstem histamine pathways influencing arousal and attention (Panula & Nuutinen, 2013; Kong *et al.*, 2023) or hypothalamic endocannabinoid pathways influencing mood, memory, and neuroprotection (de Melo Reis *et al.*, 2021).

These findings underscore the diversity of cell types and functionalities in LGN. Historically, LGN neurons were classified functionally as M, P, or K. However, our results confirm earlier suggestions (Bakken *et al.*, 2021) that the functionality of LGN neurons may be broader than traditionally held. This is particularly evident in K cells, which receive input from a diverse set of retinal ganglion cell types. These functional distinctions are important for a full understanding of the basis of primate vision. Future research can focus on correlating these transcriptomics results with anatomical and morphological data, such as through spatial transcriptomics, to draw further conclusions about the physical organization of the LGN and its rich variety of cell types.

References

Allen Institute for Brain Science (2022). Single-cell RNAseq of LGN of mouse, human, and nonhuman primate [dataset]. Available at: knowledge.brain-map.org/data/MR9M3L8BU9PCOH3BHCV/summary.

Bakken TE et al. (2018). Single-nucleus and single-cell transcriptomes compared in matched cortical cell types. *PLOS ONE* **13,** e0209648.

Bakken TE et al. (2021). Single-cell and single-nucleus RNA-seq uncovers shared and distinct axes of variation in dorsal LGN neurons in mice, non-human primates, and humans. *Elife* **10,** e64875.

Bowers CW & Schmidt CJ (1992). Mechanisms of synaptic fatigue in a developing autonomic ganglion. *Dev Biol* **154,** 410–418.

Bruntz RC, Lindsley CW & Brown HA (2014). Phospholipase D Signaling Pathways and Phosphatidic Acid as Therapeutic Targets in Cancer. *Pharmacol Rev* **66,** 1033–1079.

Butler A, Hoffman P, Smibert P, Papalexi E & Satija R (2018). Integrating single-cell transcriptomic data across different conditions, technologies, and species. *Nat Biotechnol* **36,** 411–420.

Chen W, Zhu XH, Thulborn KR & Ugurbil K (1999). Retinotopic mapping of lateral geniculate nucleus in humans using functional magnetic resonance imaging. *Proc Natl Acad Sci U S A* **96,** 2430–2434.

Cheong SK, Tailby C, Solomon SG & Martin PR (2013). Cortical-Like Receptive Fields in the Lateral Geniculate Nucleus of Marmoset Monkeys. *J Neurosci* **33,** 6864–6876.

Choudhary S & Satija R (2022). Comparison and evaluation of statistical error models for scRNA-seq. *Genome Biol* **23,** 27.

Clarke ZA, Andrews TS, Atif J, Pouyabahar D, Innes BT, MacParland SA & Bader GD (2021). Tutorial: guidelines for annotating single-cell transcriptomic maps using automated and manual methods. *Nat Protoc* **16,** 2749–2764.

Collingridge GL & Bliss TVP (1987). NMDA receptors - their role in long-term potentiation. *Trends in Neurosciences* **10,** 288–293.

Dacey D (2004). Origins of perception: Retinal Ganglion Cell Diversity and the Creation of Parallel Visual Pathways. In *Sensory Systems*, pp. 281–301.

Denison RN, Vu AT, Yacoub E, Feinberg DA & Silver MA (2014). Functional mapping of the magnocellular and parvocellular subdivisions of human LGN. *NeuroImage* **102,** 358–369.

Derrington AM & Lennie P (1984). Spatial and temporal contrast sensitivities of neurones in lateral geniculate nucleus of macaque. *The Journal of Physiology* **357,** 219–240.

Dobin A, Davis CA, Schlesinger F, Drenkow J, Zaleski C, Jha S, Batut P, Chaisson M & Gingeras TR (2013). STAR: ultrafast universal RNA-seq aligner. *Bioinformatics* **29,** 15–21.

Duffy KR, Crowder NA & LeDue EE (2012). Investigation of cytoskeleton proteins in neurons of the cat lateral geniculate nucleus. *J Comp Neurol* **520,** 186–199.

Eiber CD, Rahman AS, Pietersen ANJ, Zeater N, Dreher B, Solomon SG & Martin PR (2018). Receptive Field Properties of Koniocellular On/Off Neurons in the Lateral Geniculate Nucleus of Marmoset Monkeys. *J Neurosci* **38,** 10384–10398.

Hao Y, Stuart T, Kowalski MH, Choudhary S, Hoffman P, Hartman A, Srivastava A, Molla G, Madad S, Fernandez-Granda C & Satija R (2024). Dictionary learning for integrative, multimodal and scalable single-cell analysis. *Nat Biotechnol* **42,** 293–304.

Heynen AJ & Bear MF (2001). Long-Term Potentiation of Thalamocortical Transmission in the Adult Visual Cortex In Vivo. *J Neurosci* **21,** 9801–9813.

Hodge RD et al. (2019). Conserved cell types with divergent features in human versus mouse cortex. *Nature* **573,** 61–68.

Hodgkin AL & Huxley AF (1952). Currents carried by sodium and potassium ions through the membrane of the giant axon of Loligo. *J Physiol* **116,** 449–472.

Hubel DH & Livingstone MS (1990). Color and contrast sensitivity in the lateral geniculate body and primary visual cortex of the macaque monkey. *J Neurosci* **10,** 2223–2237.

Ichinose T & Habib S (2022). On and off signaling pathways in the retina and the visual system. *Front Ophthalmol (Lausanne)* **2,** 989002.

Javadi P, Bouskila J, Bouchard J-F & Ptito M (2015). The endocannabinoid system within the dorsal lateral geniculate nucleus of the vervet monkey. *Neuroscience* **288,** 135–144.

Jin CY, Kalimo H & Panula P (2002). The histaminergic system in human thalamus: correlation of innervation to receptor expression. *European Journal of Neuroscience* **15,** 1125–1138.

Kaplan E & Shapley RM (1982). X and Y cells in the lateral geniculate nucleus of macaque monkeys. *The Journal of Physiology* **330,** 125–143.

Kong L, Domarecka E & Szczepek AJ (2023). Histamine and Its Receptors in the Mammalian Inner Ear: A Scoping Review. *Brain Sciences* **13,** 1101.

Korsunsky I, Millard N, Fan J, Slowikowski K, Zhang F, Wei K, Baglaenko Y, Brenner M, Loh P & Raychaudhuri S (2019). Fast, sensitive and accurate integration of single-cell data with Harmony. *Nat Methods* **16,** 1289–1296.

Lasek RJ, Oblinger MM & Drake PF (1983). Molecular biology of neuronal geometry: expression of neurofilament genes influences axonal diameter. In *Cold Spring Harbor symposia on quantitative biology*, pp. 731–744. Cold Spring Harbor Laboratory Press. Available at: https://symposium.cshlp.org/content/48/731.extract [Accessed August 30, 2024].

Lause J, Berens P & Kobak D (2021). Analytic Pearson residuals for normalization of single-cell RNA-seq UMI data. *Genome Biology* **22,** 258.

Lawson SN & Waddell PJ (1991). Soma neurofilament immunoreactivity is related to cell size and fibre conduction velocity in rat primary sensory neurons. *The Journal of Physiology* **435,** 41–63.

Lein E, Borm LE & Linnarsson S (2017). The promise of spatial transcriptomics for neuroscience in the era of molecular cell typing. *Science* **358,** 64–69.

Lowe R, Shirley N, Bleackley M, Dolan S & Shafee T (2017). Transcriptomics technologies. *PLOS Computational Biology* **13,** e1005457.

Martinez-Conde S, Macknik SL & Hubel DH (2002). The function of bursts of spikes during visual fixation in the awake primate lateral geniculate nucleus and primary visual cortex. *Proceedings of the National Academy of Sciences* **99,** 13920–13925.

Maunsell JHR, Ghose GM, Assad JA, McADAMS CJ, Boudreau CE & Noerager BD (1999). Visual response latencies of magnocellular and parvocellular LGN neurons in macaque monkeys. *Visual Neuroscience* **16,** 1–14.

McInnes L, Healy J & Melville J (2020). UMAP: Uniform Manifold Approximation and Projection for Dimension Reduction. *arXiv:180203426 [cs, stat]*. Available at: http://arxiv.org/abs/1802.03426 [Accessed May 1, 2022].

de Melo Reis RA, Isaac AR, Freitas HR, de Almeida MM, Schuck PF, Ferreira GC, Andrade-da-Costa BL da S & Trevenzoli IH (2021). Quality of Life and a Surveillant Endocannabinoid System. *Front Neurosci*; DOI: 10.3389/fnins.2021.747229.

Morell P & Quarles RH (1999). The Myelin Sheath. In *Basic Neurochemistry: Molecular, Cellular and Medical Aspects. 6th edition*. Lippincott-Raven. Available at: https://www.ncbi.nlm.nih.gov/books/NBK27954/ [Accessed August 30, 2024].

Nabavi S, Kessels HW, Alfonso S, Aow J, Fox R & Malinow R (2013). Metabotropic NMDA receptor function is required for NMDA receptor-dependent long-term depression. *Proceedings of the National Academy of Sciences* **110,** 4027–4032.

Noseda R, Borsook D & Burstein R (2017). Neuropeptides and Neurotransmitters That Modulate Thalamo-Cortical Pathways Relevant to Migraine Headache. *Headache* **57 Suppl 2,** 97–111.

569 Panula P & Nuutinen S (2013). The histaminergic network in the brain: basic organization and
570 role in disease. *Nat Rev Neurosci* **14,** 472–487.

571 Park S-Y & Han J-S (2018). Phospholipase D1 Signaling: Essential Roles in Neural Stem Cell
572 Differentiation. *J Mol Neurosci* **64,** 333–340.

573 Prasad SS, Schnerch A, Lam DY, To E, Jim J, Kaufman PL & Matsubara JA (2002).
574 Immunohistochemical investigations of neurofilament M′ and αβ-crystallin in the
575 magnocellular layers of the primate lateral geniculate nucleus. *Molecular Brain Research*
576 **109,** 216–220.

577 Reid RC & Shapley RM (2002). Space and Time Maps of Cone Photoreceptor Signals in
578 Macaque Lateral Geniculate Nucleus. *J Neurosci* **22,** 6158–6175.

579 Reinagel P, Godwin D, Sherman SM & Koch C (1999). Encoding of Visual Information by LGN
580 Bursts. *Journal of Neurophysiology* **81,** 2558–2569.

581 Rousso DL, Qiao M, Kagan RD, Yamagata M, Palmiter RD & Sanes JR (2016). Two Pairs of
582 ON and OFF Retinal Ganglion Cells Are Defined by Intersectional Patterns of
583 Transcription Factor Expression. *Cell Reports* **15,** 1930–1944.

584 Ruiz-Montasell B, Aguado F, Majó G, Chapman ER, Canals JM, Marsal J & Blasi J (1996).
585 Differential Distribution of Syntaxin Isoforms 1A and 1B in the Rat Central Nervous
586 System. *European Journal of Neuroscience* **8,** 2544–2552.

587 Schiller PH & Malpeli JG (1978). Functional specificity of lateral geniculate nucleus laminae of
588 the rhesus monkey. *J Neurophysiol* **41,** 788–797.

589 Schneider KA, Richter MC & Kastner S (2004). Retinotopic Organization and Functional
590 Subdivisions of the Human Lateral Geniculate Nucleus: A High-Resolution Functional
591 Magnetic Resonance Imaging Study. *J Neurosci* **24,** 8975–8985.

592 Sherman SM & Guillery RW (2006). *Exploring the thalamus and its role in cortical function,*
593 *2nd ed*. MIT Press, Cambridge, MA, US.

594 Singh AB & Harris RC (2005). Autocrine, paracrine and juxtacrine signaling by EGFR ligands.
595 *Cellular Signalling* **17,** 1183–1193.

596 Sittig N & Davidowa H (2001). Histamine reduces firing and bursting of anterior and
597 intralaminar thalamic neurons and activates striatal cells in anesthetized rats. *Behavioural*
598 *Brain Research* **124,** 137–143.

599 Söhl G, Maxeiner S & Willecke K (2005). Expression and functions of neuronal gap junctions.
600 *Nat Rev Neurosci* **6,** 191–200.

601 Solomon SG & Lennie P (2007). The machinery of colour vision. *Nat Rev Neurosci* **8,** 276–286.

Solomon SG, Tailby C, Cheong SK & Camp AJ (2010). Linear and Nonlinear Contributions to the Visual Sensitivity of Neurons in Primate Lateral Geniculate Nucleus. *Journal of Neurophysiology*; DOI: 10.1152/jn.01118.2009.

Solomon SG, White AJR & Martin PR (2002). Extraclassical Receptive Field Properties of Parvocellular, Magnocellular, and Koniocellular Cells in the Primate Lateral Geniculate Nucleus. *J Neurosci* **22,** 338–349.

Ståhl PL et al. (2016). Visualization and analysis of gene expression in tissue sections by spatial transcriptomics. *Science* **353,** 78–82.

Stuart T, Butler A, Hoffman P, Hafemeister C, Papalexi E, Mauck WM, Hao Y, Stoeckius M, Smibert P & Satija R (2019). Comprehensive integration of single-cell data. *Cell* **177,** 1888-1902.e21.

Südhof TC (1995). The synaptic vesicle cycle: a cascade of protein–protein interactions. *Nature* **375,** 645–653.

Sun SH, Killian NJ & Pezaris JS (2024). More than expected: extracellular waveforms and functional responses in monkey LGN. 2023.11.22.568065. Available at: https://www.biorxiv.org/content/10.1101/2023.11.22.568065v2 [Accessed May 31, 2024].

Tailby C, Solomon SG & Lennie P (2008). Functional Asymmetries in Visual Pathways Carrying S-Cone Signals in Macaque. *J Neurosci* **28,** 4078–4087.

Tasic B et al. (2018). Shared and distinct transcriptomic cell types across neocortical areas. *Nature* **563,** 72–78.

Teng FYH, Wang Y & Tang BL (2001). The syntaxins. *Genome Biol* **2,** reviews3012.1.

Vries SEJ de et al. (2020). A large-scale standardized physiological survey reveals functional organization of the mouse visual cortex. *Nat Neurosci* **23,** 138–151.

Wankerl K, Weise D, Gentner R, Rumpf J-J & Classen J (2010). L-Type Voltage-Gated Ca2+ Channels: A Single Molecular Switch for Long-Term Potentiation/Long-Term Depression-Like Plasticity and Activity-Dependent Metaplasticity in Humans. *J Neurosci* **30,** 6197–6204.

Webster C (2019). *The Effects of Neurosteroids, such as Pregnenolone Sulfate and Its Receptor, TrpM3 in the Retina*. University of California, Berkeley. Available at: https://search.proquest.com/openview/a09f78561f280c7d9168af1e3c52ea02/1?pq-origsite=gscholar&cbl=18750&diss=y [Accessed August 30, 2024].

Weisskopf MG, Bauer EP & LeDoux JE (1999). L-Type Voltage-Gated Calcium Channels Mediate NMDA-Independent Associative Long-Term Potentiation at Thalamic Input Synapses to the Amygdala. *J Neurosci* **19,** 10512–10519.

White AJR, Solomon SG & Martin PR (2001). Spatial properties of koniocellular cells in the lateral geniculate nucleus of the marmoset Callithrix jacchus. *The Journal of Physiology* **533,** 519–535.

Wiesel TN & Hubel DH (1966). Spatial and chromatic interactions in the lateral geniculate body of the rhesus monkey. *Journal of Neurophysiology* **29,** 1115–1156.

Xu X, Ichida JM, Allison JD, Boyd JD, Bonds AB & Casagrande VA (2001). A comparison of koniocellular, magnocellular and parvocellular receptive field properties in the lateral geniculate nucleus of the owl monkey (Aotus trivirgatus). *J Physiol* **531,** 203–218.

Yang Y-C, Hu C-C & Lai Y-C (2015). Non-additive modulation of synaptic transmission by serotonin, adenosine, and cholinergic modulators in the sensory thalamus. *Front Cell Neurosci*; DOI: 10.3389/fncel.2015.00060.